Predicting the strength of European beech (*Fagus sylvatica* L.) boards using image-based local fibre direction data

Thomas Ehrhart [1)°] (ORCID ID: 0000-0001-9551-4714), Pedro Palma [2)*°] (0000-0003-3253-646X), Mark Schubert [3)] (0000-0002-6900-0370), René Steiger [2)] (0000-0002-0096-098X), Andrea Frangi [1)] (0000-0002-2735-1260)

[1)] ETH Zürich, Institute of Structural Engineering, Stefano-Franscini-Platz 5, 8093 Zurich, Switzerland

[2)] Empa – Swiss Federal Laboratories for Materials Science and Technology, Structural Engineering Research Laboratory, Ueberlandstrasse 129, 8600 Duebendorf, Switzerland

[3)] Empa – Swiss Federal Laboratories for Materials Science and Technology, Cellulose and Wood Materials, Ueberlandstrasse 129, 8600 Duebendorf, Switzerland

[*]corresponding author: pedro.palma@empa.ch; +41 58 765 4926

[°]Thomas Ehrhart and Pedro Palma shared joint first authorship.

Keywords

European beech, fibre direction, machine learning, strength grading, tensile strength

Abstract

Image-based local fibre direction data, generated based on the analysis of the medullary spindle pattern, was used to improve the prediction of the tensile strength parallel to the grain of European beech (*Fagus sylvatica* L.) boards. An approach to characterise the local fibre orientations in a board using a single numerical grading parameter was further developed. This parameter was used, in combination with the dynamic modulus of elasticity, to develop a regression model providing very good predictions of the experimentally determined tensile strength parallel to the grain ($R^2 = 0.84$). Subsequently, machine-learning techniques were used to improve the strength model. Non-destructive and destructive tests were performed on ($N =$) 47 boards. A data (sub-) set ($n = 36$) was used to train different machine learning techniques (Support-Vector Machines, Decision Tree, Random Forest, and Artificial Neural Network) using a 6-k cross-validation approach. The generalisation ability of the models was then assessed by a hold-out dataset ($n = 11$). The results showed that all machine-learning models presented good prediction accuracy (R^2 up to 0.88 and MAPE below 8%). The Support-Vector machine and Random Forest methods showed the best performance. The combination of experimental methods with machine learning allows for a more precise strength grading of timber and, thus, can contribute to a more resource-efficient use of wood and may open new and more demanding fields for high-level timber applications in structures.

1 Introduction

1.1 Background

Timber is a material with an excellent strength-weight ratio, the possibility of being sustainably sourced, and usually perceived as aesthetically very pleasant. However, human influence on its physical and mechanical properties is generally very limited due to the natural growth, leading to a high variability in timber properties. Without taking measures to reduce the variability, large safety factors would be needed when designing timber structures, limiting the efficiency in utilising the material. For instance, during the production of glued laminated timber (GLT) or cross laminated timber (CLT), the raw material needs to be strength graded to ensure minimum performance requirements and optimise its use. Strength grading of timber into different strength classes based on parameters obtained from non-destructive tests allows for a reduction in the material's variability and, thus, for a more efficient utilisation of the raw material. Therefore, strength grading depends mainly on the correlations between the measured (indicating) parameters and the target mechanical parameters.

1.2 State of the art

Anatomical characteristics, such as large single knots, knot clusters, bark inclusions and fibre deviations, cause the most significant reduction in the strength of timber. Regarding glued laminated timber, the tensile strength of the laminations is the key property for allocating timber boards to a certain strength class (e.g.

Ehlbeck et al., 1985; Brandner and Schickhofer, 2008; Fink, 2014). Close to knots and in knot clusters, the tensile strength of a board is reduced due to local deviations to the mainly longitudinal fibre direction and due to the reduction in cross-sectional area available for these fibres in the presence of knots. This results in non-uniform stress distributions in these cross sections, especially in case of eccentric knots (Foley, 2001). Limits regarding the knot size are provided for different grades in current strength grading standards, such as DIN 4074-1 (2012), for strength grading of coniferous sawn timber, and DIN 4074-5 (2008), for strength grading of deciduous sawn timber. For boards with fewer and smaller knots, the influence and importance of other characteristics increases. In particular, the local fibre direction becomes more important. DIN 4074-1 (2012) and DIN 4074-5 (2008) specify threshold values of this grading parameter that correspond to the various grades too. The local fibre direction also has a high influence in the strength of finger joints in beech wood laminations (Aicher et al., 2001). The detection and quantification of the fibre direction is much more complex than the determination of the size of knots and is particularly relevant to machine grading (Ridley-Ellis et al., 2016). On the one hand, the fibre direction is often difficult to detect with the naked eye; on the other hand, the fibre direction changes continuously along the length and width of a board. To overcome these problems, procedures and instruments have been developed to automatically evaluate the fibre direction (Schlotzhauer et al. 2018).

Multiple physical principles are employed to evaluate the fibre direction. Among them are the dielectric properties of wood (Baradit et al., 2006; Denzler and Weidenhiller, 2015; Norimoto and Yamada 1972), the electrical field strength (Cramer and McDonald, 1989; Norton et al., 1974; Steele et al., 1991), the thermal conductivity (Belkacemi et al., 2016; Daval et al., 2015; Krapez et al., 1996), and the so-called tracheid effect (Matthews and Beech, 1976; Matthews and Soest, 1986; Metcalfe and Dashner, 2002; Nyström, 2003; Sarén, et al., 2006; Simonaho et al., 2004; Soest, 1997). The method based on the tracheid effect has been frequently used in descriptions and models of timber and its anatomical structure (Briggert et al., 2016; Foley, 2001; Lukacevic and Füssl, 2014). The tracheid effect has been used to improve the strength grading of coniferous timber (Brännström et al., 2008; Olsson et al., 2013; Olsson and Oscarsson, 2017; Viguier et al., 2015, 2017). More recently it has also been applied successfully to fibre orientation measurements on hardwoods (Besseau et al., 2020), on beech veneers to estimate the modulus of elasticity of LVL (Viguier et al. 2018), and to strength grading of oak (Olsson et al., 2018).

The vast majority of the mentioned investigations focused on coniferous timber species, mainly Norway spruce (*Picea abies* (L.) Karst.). For European beech (*Fagus sylvatica* L.) timber, significantly fewer studies are available. In Switzerland, Germany, and Austria, European beech amounts to 18, 15, and 10% of the total forest stock, respectively, corresponding to shares between 50 and 80% of the hardwood stock in these countries (FOEN, 2018; Sauter and Breinig, 2016). European beech timber is also among the European native species with the highest strength and stiffness properties. Compared to timber from coniferous trees, European beech timber exhibits significantly fewer knots and knot-free boards predominate in high strength classes. Consequently, the strength grading parameter fibre direction is of utmost importance.

Ehrhart et al. (2018a) presented a non-contact method for the identification, quantification, and documentation of the fibre direction in European beech timber based on the analysis of the medullary rays. Making use of image analysis techniques, the spindle pattern formed by the medullary rays was used to predict the fibre direction in European beech boards. Curti et al. (2018) adapted this method to investigate the effect of fibre direction on cutting forces and chip geometry during machining of beech timber in the fibre-saturated state.

To further increase the reliability and utilisation efficiency of timber in general, improved machine grading procedures are required to measure various grading parameters at high speed, with greater accuracy and precision. In general, the correlation between the measured grading parameters and the structural properties is performed using simple linear or multi-linear correlations (Ehlbeck et al., 1985; Fink, 2014), neglecting that the structure of timber is complex and that these correlations are often non-linear. Machine learning techniques are particularly suited to overcome challenges related to finding patterns in complex systems. These data-driven approaches are able to identify hidden patterns in data of different type and create classification and predictive models (Fathi et al., 2020; Schubert and Kläusler, 2020). Combining machine-learning techniques with non-destructive optical and digital image analysis methods is therefore a promising strategy for grading high-strength timber boards with few obvious visual defects. These advanced grading techniques can be further complemented with mechanical constitutive models, which

establish the relation between material parameters and external loads (e.g. Sarnaghi and van de Kuilen, 2019), leading to hybrid strength grading approaches.

1.3 Objective, scope, and overview

The objective of this study was to develop a model to improve the prediction of the tensile strength of European beech (*Fagus sylvatica* L.) boards without obvious visual defects. The developed model considers the measured dynamic modulus of elasticity and new information on the fibre direction, obtained through a non-destructive and non-contact method developed by Ehrhart et al. (2018a). Different machine learning techniques are applied and their potential for maximising the prediction quality of the models is evaluated.

2 Materials and methods

2.1 Overview

This study was based on 47 flat sawn planed beech boards supplied by four Swiss sawmills. The dimension of the boards was $l_b \times w_b \times t_b = 3000 \times 160 \times 25$ mm^3. The thickness of the beech laminations $t_b = 25$ mm is significantly smaller than usual thicknesses of softwood laminations (up to 40 mm), but this is due to delamination problems arising when beech laminations thicker 30 mm are used (Ohnesorge et al. 2010) for glulam production.The average moisture content of the boards at the time of testing was $\omega = 8 \pm 2\%$. This moisture content corresponds to an environment with 24 °C and 35% relative humidity, which is not uncommon in offices and residential buildings and also corresponded to the expected environmental conditions in the labs where the tests were performed. Since the focus of this study was on improving the grading of high strength boards, only boards free of knots, bark inclusions and other obvious structural characteristics affecting the tensile strength parallel to the grain were considered. The wide faces of the boards were mostly parallel to the longitudinal-tangential plane of the wood. In such knot-free boards, the influence of fibre orientation on the tensile strength becomes more important. Ehrhart et al. (2018a) have shown that the medullary ray spindle pattern, which is clearly visible on the face sides, can be used to assess the local fibre orientation. About 75% of the 47 boards were comprehensively photographed, documented, and tested to failure in tension parallel to the grain by Ehrhart et al. (2016b). The other 25% of the boards were analysed and the density, the dynamic MOE, the surface photographs and the experimental tensile strength were documented by Jungo (2016). The data sets collected by Ehrhart et al. (2016a) and Jungo (2016) were combined and subsequently randomly split into two data sets: a training or calibration data set (used to fit models) and a test data set (used to evaluate the models). The training data set consisted of 36 boards (77%) and the test data set of 11 boards (23%). The total number of boards used in this study is limited, but was shown to be adequate to assess the ability of the proposed method of using image-based local fibre direction data to very significantly improve the prediction of the tensile strength of European beech boards.

2.2 Strength grading parameters measured using non-destructive methods

2.2.1 Density and dynamic modulus of elasticity

The devices *Brookhuis MTG Timber Grader* and *Microtec ViScan* were used to determine the density and the dynamic modulus of elasticity of the beech boards (Ehrhart (2019) showed that the two systems provide almost identical results). The dynamic modulus of elasticity E_{dyn} was calculated using Equation 1, based on the first longitudinal eigenfrequency f_e, the density ρ and the length l_b of the board.

$$E_{dyn} = 4 \cdot f_e^{\,2} \cdot l_b^{\,2} \cdot \rho \qquad (1)$$

The statistical parameters of the dynamic modulus of elasticity and density are summarised in Table 1 for both the training ($n = 36$) and the test ($n = 11$) data sets. The range of density is wider for the training data set (647 – 817 kg/m^3) than for the test data set (671 – 759 kg/m^3). However, the mean values of density at a moisture content of $\omega = 8 \pm 2\%$ ($\rho_{8,mean}$) and the coefficients of variation (cov) of both data sets agree well (726 and 710 kg/m^3 and 0.05 and 0.04, respectively). Similar values of densities of European beech are reported by Frühwald and Schickhofer (2005), Frese (2006), Hübner (2013), and Westermayr et al. (2018).

The range of the dynamic modulus of elasticity is also wider for the training (12805 – 23371 MPa) than for the test data set (13613 – 20791 MPa) and the mean value of the training data set is slightly higher than that

of the test data set (16520 and 16291 MPa, respectively). Frese (2006) reported a range of 9656 – 20613 MPa and a mean value of 14506 MPa.

Table 1 Statistical parameters for the density ρ, dynamic modulus of elasticity E_{dyn}, static modulus of elasticity $E_{t,0}$ and tensile strength parallel to the grain $f_{t,0}$ of the training and test data sets ($\omega = 8 \pm 2\%$.).

	Parameter	Symbol	Unit	*n** [-]	Min	Mean	Max	Cov [-]
All boards	Density	ρ	kg/m³	47	647	722	817	0.05
	Dynamic modulus of elasticity (MOE)	E_{dyn}	MPa		12805	16466	23371	0.13
	Static MOE	$E_{t,0}$	MPa		12102	15479	20457	0.12
	Tensile strength	$f_{t,0}$	MPa		42.2	88.5	132	0.25
Training data set**	Density	ρ	kg/m³	36	647	726	817	0.05
	Dynamic MOE	E_{dyn}	MPa		12805	16520	23371	0.14
	Static MOE	$E_{t,0}$	MPa		12102	15428	20457	0.11
	Tensile strength	$f_{t,0}$	MPa		42.2	85.4	132	0.25
Test data set**	Density	ρ	kg/m³	11	671	710	759	0.04
	Dynamic MOE	E_{dyn}	MPa		13613	16291	20791	0.14
	Static MOE	$E_{t,0}$	MPa		12288	15646	18985	0.13
	Tensile strength	$f_{t,0}$	MPa		49.5	90.4	119	0.26

* Number of boards.
** The data was split into two data sets: one for training (i.e. calibrating) the models and one for testing the fitted models.

2.2.2 Local fibre direction

The local fibre direction was identified, quantified, and documented using the non-destructive and non-contact method developed by Ehrhart et al. (2018a). This method assumes that the medullary rays and the annual rings form corridors, along which the wood fibres run and, thus, are a proxy for the fibre direction. Due to the low shear strength of European beech wood in the longitudinal-radial plane (Ashby et al., 1985), the spindles formed by the medullary rays were found to be an excellent indicator for the critical fibre direction, i.e., the fracture path developing in destructive tension tests.

The two opposite face sides of the middle 2000 mm (= tested free-length of the boards in the tension tests, see Subsection 2.3) of the 3000 mm long boards were documented by taking four consecutive photographs of 500 mm-long segments. Hence, eight photographs were taken of each board. Figure 1a shows a part of one of the resulting digital photographs. Subsequently, these digital images were batch-processed to isolate and identify the medullary ray spindles using the program *Adobe Photoshop 2020*. The steps of this pre-processing were: i) smart sharpening (amount: 500%, radius: 7.5 pixels); ii) convert mode (to grayscale); iii) apply a cut-out filter (levels = 4, edge simplicity = 1; edge fidelity = 3); set a threshold (level: 75). Each file covers a board length of 500 mm and the resulting PNG-files have an approximate size of 100 kB (the original size of the photograph was approximately 5 MB). The black and white image showing the isolated medullary ray spindles of the photograph in Figure 1a is shown in Figure 1b.

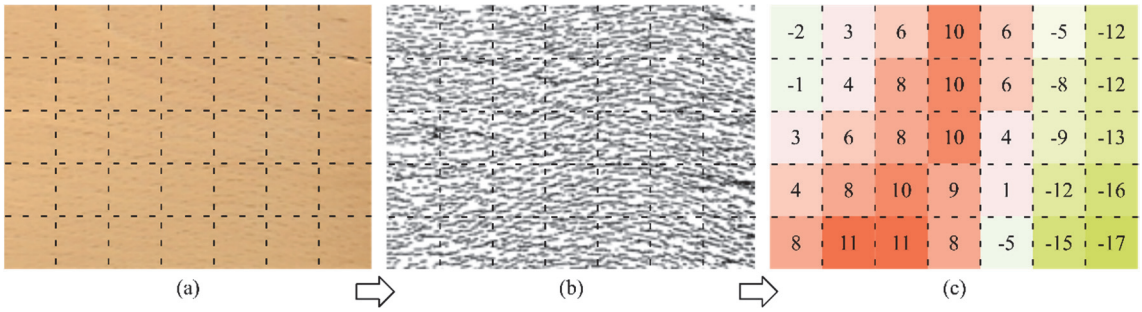

Figure 1 Non-contact determination of the fibre direction: based on a photograph (a), the medullary ray spindles are isolated (b), and their coordinates and geometrical properties are documented. Post processing of the resulting data allows generating discretised fields of fibre direction, e.g. average local angle between the fibre directions and the longitudinal direction of the boards (c).

The black and white PNG-images were analysed using the program *ImageJ* (Image Processing and Analysis in Java) (Schindelin et al., 2012). By applying a threshold, the medullary ray spindles were identified as objects (an example based on an image of segment no. 4 of board no. 1004 is shown in Figure 2a). Subsequently, a list of the properties of all objects was generated, including: coordinates x_M and y_M of the centre of mass (in pixels); area A (in pixels); circularity c (calculated using Equation 2, in which P is the perimeter of the object in pixels); and angle α between the major axis of an ellipse fitted to the object and the longitudinal direction of the board (in degrees). The angle α was measured in counter-clockwise direction, objects with angles above 90° were considered as having negative orientations, i.e. $\alpha = \alpha_{measured}$ - 180 (Figure 2b).

$$c = 4 \cdot \pi \cdot \frac{A}{P^2} \quad (2)$$

Only objects that represent medullary ray spindles should be considered in the analysis of the field of fibre direction. Thus, objects resulting from dirt, markings or other sources were removed by filtering the resulting object list. The filtering criteria to define valid objects were: object area A between 50 and 500 pixels (approximately 0.45 to 4.50 mm^2); circularity c between 0.02 and 0.60 and; absolute orientation α below 45°. Fields of local fibre direction were then obtained by discretising the boards into surface elements with a size of ($e \times e$ =) 20 × 20 mm^2 and calculating the average fibre direction in each element taking into account the results for both face sides. This element size was chosen as a compromise between enough resolution to reliably detect fibre orientation and avoiding "empty" grid elements, for which no fibre orientation could be determined. If less than five elements were present in an element, no fibre direction was calculated. Figure 1c presents the resulting field of fibre direction for the segment shown in Figure 1a and b.

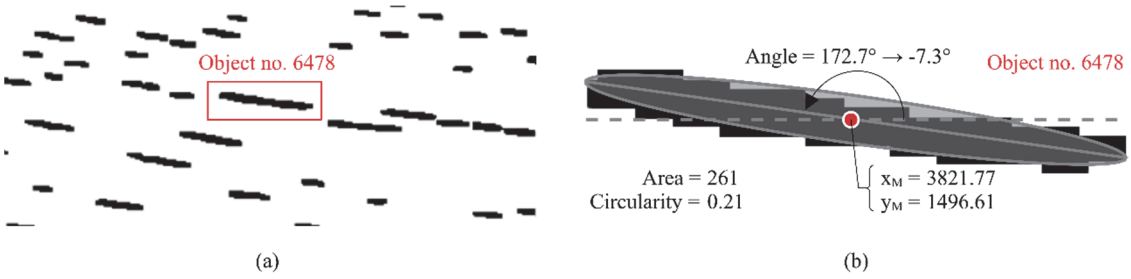

Figure 2 Detail image of board no. 1004, segment no. 4, after isolation of the medullary ray spindles (a). As an example, information on the coordinates, the area, the circularity, and the angle of object no. 6478 are shown (b).

2.3 Tensile strength parallel to the grain measured in tension tests to failure

2.3.1 Test set-up

The tensile strength parallel to the grain of the European beech boards was determined in accordance with EN 408 (2012), using a *Gehzu 850* horizontal testing machine (Figure 3). The boards had a total length l_b = 3000 mm, but the free testing-length between the clamps (Figure 3b) was l_{test} = 2060 mm, which was very approximately the part of the boards for which the local fibre direction was analysed (see Subsection 2.2.2). In addition to the tensile strength parallel to the grain $f_{t,0}$, also the static modulus of elasticity parallel to the grain $E_{t,0}$ was determined in accordance with EN 408 (2012), based on

measurements performed using linear variable differential transformers (LVDT) attached to both edge faces of the boards (Figure 3c).

(a) (b) (c)

Figure 3 Tensile testing machine *Gehzu 850*, used to determine the tensile strength parallel to the grain $f_{t,0}$ (a). Vertical hydraulic jacks that apply the clamping pressure and horizontal load cells to measure the applied tensile force (b). Displacement transducers on the edge faces, used to determine the static modulus of elasticity parallel to the grain $E_{t,0}$ (c).

2.3.2 Test results

The statistical parameters of the tensile strength and static MOE parallel to the grain are summarised in Table 1 for the training ($n = 36$) and the test ($n = 11$) data sets. The range of tensile strength is slightly wider for the training data set (42.2 – 132 MPa; cov = 0.25) compared to the test data set (49.5 – 119 MPa; cov = 0.26). The mean value of tensile strength is about 6% lower in the training data set ($f_{t,0,mean} = 85.4$ MPa) compared to the test data set ($f_{t,0,mean} = 90.4$ MPa). Similarly, a wider range but a slightly lower mean value of the static MOE were found for the training data set ($E_{t,0,mean} = 15428$ MPa) compared to the test data set ($E_{t,0,mean} = 15646$ MPa).

Table 2 Tensile strength parallel to the grain of European beech boards reported in other studies.

Study	**Remark**	**Tensile strength parallel to the grain [MPa]**				
		n* [-]	**Min**	**Mean**	**Max**	**Cov [-]**
Glos and Lederer (2000)	-	219	11.3	48.7	117	0.46
Frühwald and Schickhofer (2005)	-	112	16.7	62.3	115	0.40
Blaß et al. (2005)	-	354	-	68.1	-	0.50
Plos et al. (2018)	-	191	19.1	72.1	142	0.38
Weidenhiller et al. (2019)	Training / test data sets	21/20	-	58.7/51.3	-	0.46/0.55
Ehrhart (2019)	All boards	294	4.3	63.4	132	0.65
This study	tKAR ≤ 0.05	170	26.1	78.2	132	0.29
	tKAR = 0 (only boards free of knots were used)	47	42.2	86.6	132	0.25

* Number of tests.

The results of previous tensile testing campaigns on European beech boards are summarised in Table 2. The tensile strengths were between 4.3 and 142 MPa (Blaß et al., 2005; Ehrhart, 2019; Frühwald and Schickhofer, 2005; Glos and Lederer, 2000; Plos et al., 2018; and Weidenhiller et al., 2019). Since only flat sawn boards free of knots were investigated in this study, the variation of results is significantly lower. No strength values below 40 MPa were observed. Nevertheless, the maximum values in the data sets are close to those reported in other studies (Table 2).

2.3.3 Failure patterns

As described in Ehrhart et al. (2018a), the dominating failure mode was shear failure along the spindles formed by the medullary rays. As an example of a board with the spindles formed by the medullary rays running mostly parallel to the x-axis, i.e. the longitudinal axis of the board, a segment of board no. 3002 is shown in Figure 4a. The objects identified in this board segment are shown in Figure 4b, where the almost horizontal orientation of the spindles is even clearer. The stain at the bottom part of the image is not considered in the calculation of the fibre direction matrix due to its circularity (> 0.6) and the orientation of the main axis of the fitted ellipse (> 45°) (see filtering criteria in Subsection 2.2.2). Failure cracks created in the tension tests are shown in Figure 4c. It can be seen that these cracks run mostly parallel to the x-axis, meaning that the fibres are quite straight ($\alpha \approx 0$). Due to the small fibre inclination, a relatively high tensile strength of $f_{t,experimental} = 112$ MPa was observed with board no. 3002.

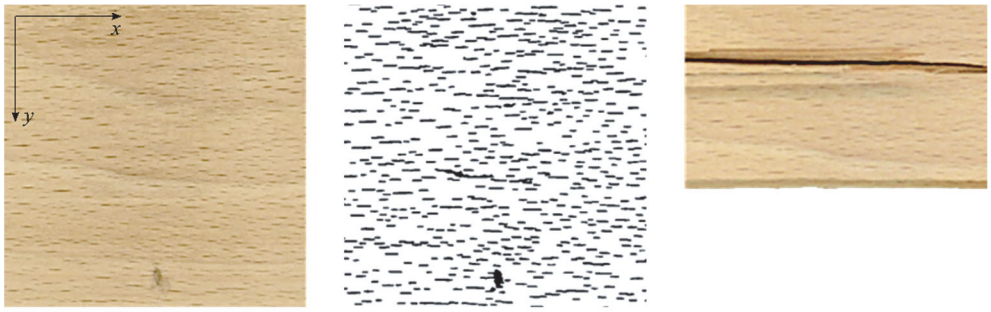

(a) (b) (c)

Figure 4 Detail image of a segment of board no. 3002, the spindles formed by the medullary rays running mostly parallel to the longitudinal axis of the board (a), identified objects (b) and fracture path in the same segment (c). This board exhibited a tensile strength of 112 MPa in the tensile test to failure.

As an example of a board with a higher fibre inclination, a segment of board no. 2058 is shown inFigure 5. Both in the original image (Figure 5a) and the image showing the objects (Figure 5b), a negative inclination of the spindles ($\alpha \approx -15°$) is clearly seen. The actual fibre direction, revealed by the failure pattern shown in Figure 5c, agrees well with this observation. A significantly lower tensile strength of $f_{t,0,experimental} = 42$ MPa was observed in the tensile test.

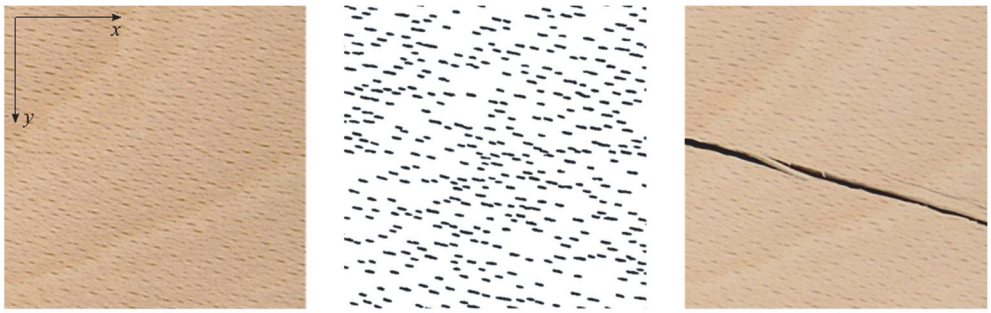

(a) (b) (c)

Figure 5 Detail image of a segment of board no. 2058, with the spindles formed by the medullary rays running mostly at an angle of 15° to the longitudinal axis of the board (a), identified objects (b) and fracture path in the same segment (c). This board exhibited a tensile strength of 42 MPa in the tensile test to failure.

2.4 Numerical methods

2.4.1 Data-fitting methods

The regression parameters were calibrated by minimising the residual sum of squares (RSS) between the estimated and the experimentally determined tensile strengths. This was done using the generalised reduced gradient (GRG) nonlinear solver implemented in MS Excel 2016. Only the training dataset (36 boards) was used in the model calibration.

2.4.2 Machine-learning techniques

The main objective of using machine-learning techniques is to properly adjust important hyperparameters of the algorithms and to avoid over-fitting, in order to achieve a good generalisation with respect to the

unseen test data (Mansfield et al., 2007). Thus, the choice of a proper experimental methodology is crucial. Therefore, as mentioned before, the data set ($N = 47$) was divided in: a training data set ($n = 36$) and a test data set ($n = 11$). The training data set was used to identify and adjust important model hyperparameters by applying a ($k =$) 6-fold cross-validation approach (Kohavi, 1995). Cross-validation is a resampling procedure used to effectively evaluate machine-learning models on a limited data set (Kohavi, 1995). In the process of cross validation, one part of the training data set ($n = 36$) was set as the validation data set, while the remaining $k–1 = 5$ parts were used as the training data set.

After training the machine-learning algorithms using the cross-validation method, the generalisation ability was assessed with the test data set (hold-out evaluation) based on the accuracy measures: coefficient of determination (R^2); root mean square error (RMSE) and; mean absolute percentage error (MAPE). The results from this evaluation serve as a quality measure (generalisation ability) for these models. Typical MAPE values for performance evaluation are categorised as follows (Lewis, 1982): MAPE ≤ 10% corresponds to a 'high accuracy prediction'; 10% < MAPE ≤ 20% corresponds to a 'good prediction'; and 20 < MAPE ≤ 50% corresponds to a 'reasonable prediction'. A MAPE above 50% indicates an 'inaccurate prediction'. The input parameters for the machine-learning techniques were the same that were used in the developed physically-based model.

Deep learning approaches, e.g. convolutional neural networks, would be particularly suited to predict the tensile strength based solely on images of the boards, but require extremely large data sets and are computationally intensive. Therefore, shallow machine-learning algorithms were used instead. Shallow algorithms require the data to be described by pre-defined features, which in this case are the grading parameters and the local fibre direction.

The machine learning techniques applied in this study were *Support-Vector Machines* (e.g. Vapnik, 1995), *Decisions Tree* (e.g. Kotsiantis, 2013), *Random Forest* (e.g. Breiman, 2001), and *Artificial Neural Network* (e.g. Hinton and Salakhutdinov, 2006).

Introduced by Vapnik (1995), *Support-Vector Machines* are supervised learning models for classification and regression. Since Support-Vector Machine regression relies on kernel functions, it is considered a nonparametric technique. In this study, the scaling factor, i.e., the kernel scale, and the cost function were optimised using sequential minimal optimisation (SMO). *Decision Trees* build regression or classification models in the form of a tree structure (Kotsiantis 2013). Thereby, the data is split into at least two homogeneous sets (also called sub-populations) based on the most significant features of the input variables. An associated Decision Tree, featuring decision nodes and leaf nodes, is incrementally developed. Decision Trees are precursors to Random Forests (Kotsiantis, 2013). Operated by constructing a multitude of decision trees, a *Random Forest* is an ensemble learning method for (e.g.) classification and regression. Thereby, each tree is generated using a random variable subset from the candidate's predictor variables and a random subset of data, generated by means of a bootstrap (Breiman, 2001). *Artificial Neural Networks* comprise three functional parts (Hinton and Salakhutdinov 2006): i) input layer; ii) hidden layers; and iii) an output layer. The hidden part can consist of many layers that enable multi-level and non-linear operations (Hinton and Salakhutdinov, 2006). The interconnections between nodes, the parameters that represent the strengths of the interconnections (weights), and the activation function, which is a nonlinear function that converts the weighted sum of the input signals to output at each node, are important features for the performance of the network and are adjusted through learning (LeCun et al., 2015). The learning process for updating weights is called "training", which occurs in an iterative way. During each optimisation step, the weights are adjusted in order to reduce the difference between the prediction and the measured activity (Hinton and Salakhutdinov, 2006).

All algorithms were programmed in MATLAB R2018b (using the statistics and machine learning toolbox). The hyperparameters of the Support-Vector Machines, Decision Trees, and *Random Forests*were optimised using Bayesian optimisation (Snoek et al., 2012). The optimal configuration, i.e. the decision about the type of training algorithm, learning rate, activation function (e.g. radial basis, tanh, ReLU) and number of layers and neurons per layer for the artificial neural network, was obtained by a trial and error approach until no further improvement could be achieved. A detailed mathematical description of the algorithms has been presented by Bishop (2006).

3 Development and evaluation of strength models

3.1 Overview

This study focused on grading high-strength European beech boards free of knots. Thus, knot-related parameters, such as the single knot (DEB) and the knot cluster (DAB) parameter, or the knot area ratio (KAR) and the total knot area ratio (tKAR), could not be used in the models to estimate the tensile strength.

The potential of using the board density (ρ) and the dynamic modulus of elasticity (E_{dyn}) as grading parameters for the tensile strength parallel to the grain ($f_{t,0}$) of beech boards was investigated in several studies (Glos and Lederer, 2000; Frühwald, et al., 2003;, Frühwald and Schickhofer, 2005; Plos et al., 2018; Weidenhiller et al., 2019; Ehrhart, 2019). The reported coefficients of determination between the density and the tensile strength parallel to the grain, i.e. $R^2(\rho,f_{t,0})$, were consistently very low ($R^2 < 0.20$) (Table 3). Low coefficients of determination of $R^2 = 0.06$ were also found in the present study (Figure 6a).

Table 3 Coefficients of determination R^2 between the potential strength grading parameters density (ρ) and dynamic MOE (E_{dyn}) and the target parameter tensile strength parallel to the grain ($f_{t,0}$) reported in previous studies (listed in the first column of the table) and found for the data training and test sets used in the present study.

	Remark	***n* [-]**	**$R^2(\rho, f_{t,0})$**	**$R^2(E_{dyn}, f_{t,0})$**
Glos and Lederer (2000)	-	219	0.02	-
Frühwald, et al. (2003)	-	70	0.17	0.19
Frühwald and Schickhofer (2005)	*	202	0.03	0.26
Plos et al. (2018)	-	191	0.05	-
Weidenhiller et al. (2019)	Training / test data	21/20	-	0.62/0.57
Ehrhart (2019)	All boards	294	0.00	0.27
	tKAR ≤ 0.05	170	0.03	0.10
Present study	**All boards**	**47**	**0.06**	**0.48**
	Training data set**	36	0.07	0.48
	Test data set**	11	0.10	0.53

* Global coefficients of determination for three hardwood species (European beech (*Fagus sylvatica* L.), oak (*Quercus robur* L.), and ash (*Fraxinus excelsior* L.)).
** For training and testing of the model, the data was split into two data sets.

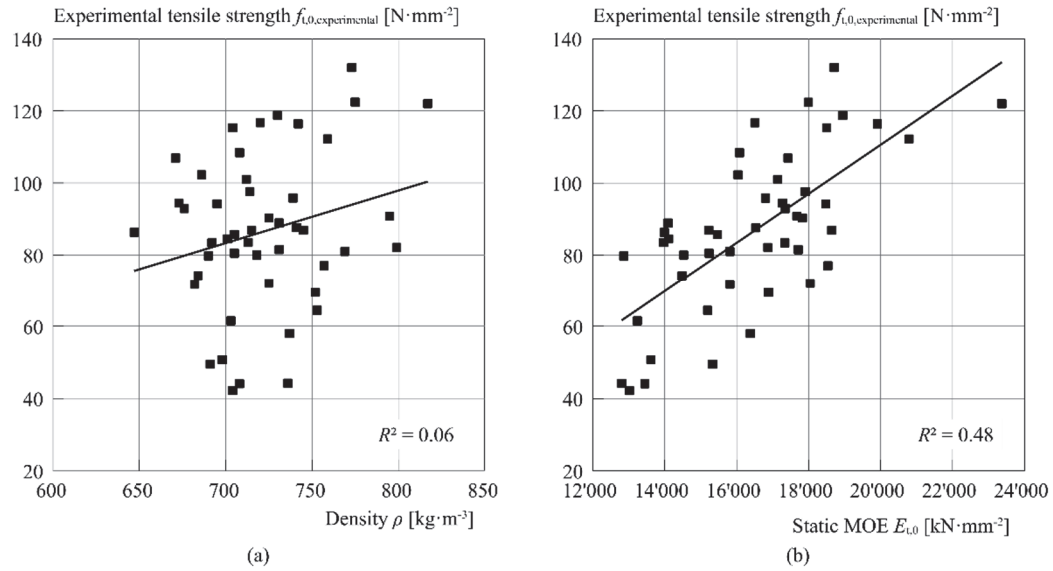

Figure 6 Correlation of potential grading parameters density (a; $R^2 = 0.06$) and dynamic modulus of elasticity (b; $R^2 = 0.48$) with the target parameter tensile strength parallel to the grain ($f_{t,0}$).

The coefficients of determination for a linear correlation between the dynamic MOE and the tensile strength parallel to the grain reported in the literature are much more diverse (Table 3). While Ehrhart (2019), Frühwald et al. (2003), and Frühwald and Schickhofer (2005) reported relatively low coefficients of determination (R^2 between 0.19 and 0.27), Weidenhiller et al. (2019) observed much higher coefficients of determination ($R^2 \approx 0.60$). In this study, a coefficients of determination between the dynamic MOE and the tensile strength parallel to the grain, i.e., $R^2(E_{dyn}, f_{t,0})$, of 0.48 (Figure 6b) was found.

3.2 Sub-model to estimate the minimum local tensile strength of a board

As described above, the fibre orientation within a board is not constant. It changes continuously both along the longitudinal as well as along the transverse axis of a board. Generally, the tensile strength is locally reduced in areas with high fibre inclination. However, not only the tensile strength but also the static MOE is smaller for elements with high fibre inclination. Consequently, the stresses in a cross section are distributed depending on the stiffnesses of its elements and failure will not necessarily occur in the element with the highest fibre inclination. To this into account, a sub-model to calculate the minimum local tensile strength of a board min($f_{t,ij}$) is implemented. A preliminary study based on this approach was presented by Ehrhart et al. (2018b). The minimum local tensile strength corresponds to the external stress that leads to the failure of the first element.

For calculating min($f_{t,ij}$), the local fibre orientation matrices (see Subsection 2.2.2) are taken into account. Constant strain across each cross section is assumed, i.e. the stresses within a cross section are distributed according to the local static MOE of each element in the cross section. The local MOE used herein ($E_{t,ij}$) is calculated based on the local fibre direction α_{ij} of each element (Figure 7a) using the Hankinson model (Equation 3) (Hankinson, 1921). The resulting matrix of $E_{t,ij}$ has a size of m (= w_b / e = 160 mm / 20 mm = 8) × n (= $l_{relevant}$ / e = 2000 mm / 20 mm = 100).

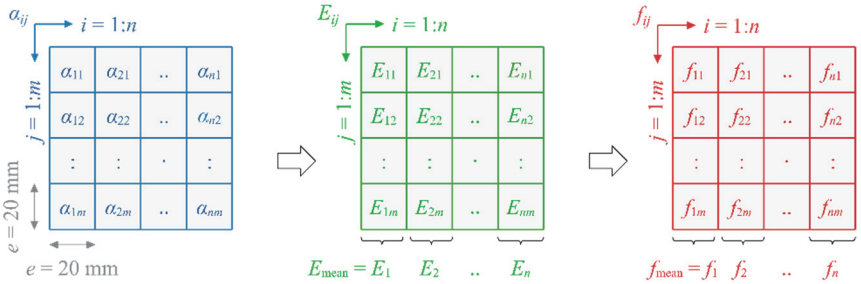

Figure 7 Discretisation of the boards into elements ij of $e \times e$ = 20 mm × 20 mm. For each element, the fibre direction (a), the estimated local static modulus of elasticity $E_{t,ij}$ (b), and the estimated local tensile strength $f_{t,ij}$ (c) are determined.

In Equation 3, the local fibre direction (α_{ij}), the reference static MOE parallel ($E_{t,0,ref}$) and perpendicular to the grain ($E_{t,90,ref}$) as well as the exponent (a) are considered. Subsequently, the average MOE of each cross section ($E_{t,i}$) was calculated. The exponent (a) was calibrated through a data-fitting procedure on the training data set (see Subsection 3.4).

$$E_{t,ij} = \frac{E_{t,0,ref} \cdot E_{t,90,ref}}{E_{t,0,ref} \cdot \sin^a(\alpha_{ij}) + E_{t,90,ref} \cdot \cos^a(\alpha_{ij})} \quad (3)$$

The matrix of local tensile strengths $f_{t,ij}$ (Figure 1c), i.e. the external stress that would cause failure in the element e_{ij}, was calculated considering the local fibre direction α_{ij}, the local stiffness $E_{t,ij}$, and the mean stiffness of the cross section i using Equation 4. The reference tensile strength parallel ($f_{t,0,ref}$) and perpendicular to the grain ($f_{t,90,ref}$) were chosen according to Wagenführ (2006). The calibration parameter b was determined through a data-fitting procedure on the training data set (see Subsection 3.4).

$$f_{t,ij} = \frac{f_{t,0,ref} \cdot f_{t,90,ref}}{f_{t,0,ref} \cdot \sin^b(\alpha_{ij}) + f_{t,90,ref} \cdot \cos^b(\alpha_{ij})} \cdot \frac{E_{t,ij}}{E_{t,i}} \quad (4)$$

In the modelling of the tensile strength ($f_{t,estimated}$), the grading parameter E_{dyn} and the grading parameter min($f_{t,ij}$) are taken into account. The latter one allows considering the influence of the local fibre orientation. In accordance with previous studies (Frühwald and Schickhofer, 2005; Blaß et al., 2005; Plos et al., 2018),

no significant influence of the density on the tensile strength could be determined. Hence, this grading parameter is not considered in the developed model.

3.3 Sub-model to estimate the tensile strength parallel to the grain of a board

The model to estimate the tensile strength parallel to the grain of a board is based on two independent variables E_{dyn} and $\min(f_{t,ij})$. It has been shown that the dynamic modulus of elasticity E_{dyn} exhibits a medium linear correlation with the tensile strength (R^2 (X_1, $\ln(f_{t,0})$) = 0.48; Figure 6b) (correlation categorisation based on the JCSS Probabilistic Model Code (JCSS, 2006): 0.8 ↔ high correlation, 0.6 ↔ medium correlation, 0.4 ↔ low correlation, 0.2 ↔ very low correlation). The independent variable $\min(f_{t,ij})$ represents the minimum of the estimated local tensile strengths of each cross section and is related to the local fibre orientation as described in Subsection 3.2 and Figure 7. The model assumes a multilinear correlation between the variables E_{dyn} and $\min(f_{t,ij})$ and the logarithm of the estimated tensile strength ($f_{t,estimated}$) and includes three calibration parameters (C_i) (Equation 5).

$$\ln\left(f_{t,0,estimated}\right) = C_0 + C_1 \cdot E_{dyn} + C_2 \cdot \min(f_{t,ij}) \tag{5a}$$

$$f_{t,0,estimated} = e^{\left(C_0 + C_1 \cdot E_{dyn} + C_2 \cdot \min(f_{t,ij})\right)} \tag{5b}$$

$$f_{t,ij} = \frac{f_{t,0,ref} \cdot f_{t,90,ref}}{f_{t,0,ref} \cdot \sin^b(\alpha_{ij}) + f_{t,90,ref} \cdot \cos^b(\alpha_{ij})} \cdot \frac{\frac{E_{t,0,ref}}{E_{t,90,ref}}}{\frac{E_{t,0,ref}}{E_{t,90,ref}} \cdot \sin^a(\alpha_{ij}) + \cos^a(\alpha_{ij})} \Big/ \frac{1}{m} \cdot \sum_{j=1}^{m} \left(\frac{\frac{E_{t,0,ref}}{E_{t,90,ref}}}{\frac{E_{t,0,ref}}{E_{t,90,ref}} \cdot \sin^a(\alpha_{ij}) + \cos^a(\alpha_{ij})} \right) \tag{6}$$

3.4 Calibration and testing of the model

The model to estimate the tensile strength of a board, resulting from combining the sub-models described in the previous subsections, is presented in Equations 5 and 6. Thereby, E_{dyn} is the measured dynamic MOE (see Subsection 3.3), a_{ij} is the computed local fibre orientation and m is the number of cross sections in the considered discretisation of the board (see Subsection 3.2). The calibration parameters of the model are the exponents a and b (model to estimate the minimum local tensile strength of a board, Subsection 3.2) and C_0, C_1, and C_2 (model to estimate the tensile strength of a board, Subsection 3.3). To ensure that the calibration parameters remain within reasonable values, i.e. that they make physical sense, the threshold values presented in Table 4 were enforced during the calibration procedure.

Table 4 Regression coefficients C_i, the exponents for the dynamic modulus of elasticity (a) and the tensile strength (b) used in the model. The reference tensile strengths parallel ($f_{t,0,ref}$) and perpendicular to the grain ($f_{t,90,ref}$) and the ratio $E_{t,0,ref}/E_{t,90,ref}$ were assumed according to Wagenführ (2006).

	Characteristic	Symbol	Calibration interval	Value (calibrated or predefined[a])	Confidence interval[b]
Parameters related to dynamic MOE (Equation 3)	Ratio MOE parallel / perpendicular to the grain	$E_{t,0,ref}/E_{t,90,ref}$	n.a.	30[a]	n.a.
	MOE exponent	a	[1; 3]	1.6	± 0.27
Parameters related to tensile strength (Equation 4)	Tensile strength parallel to the grain	$f_{t,0,ref}$	n.a.	180 MPa[a]	n.a.
	Tensile strength perpendicular to the grain	$f_{t,90,ref}$	n.a.	7 MPa[a]	n.a.
	Tensile strength exponent	b	[1; 3]	2.5	± 0.40
Regression parameters (Equation 5)	Intercept	C_0	[-3; 3]	1.91	± 0.29
	MOE parameter	C_1	[0; 10^{-3}]	$5.06 \cdot 10^{-5}$	$\pm 2.23 \cdot 10^{-5}$
	Tensile strength parameters	C_2	[0; 1]	0.0121	± 0.0039

[a] Predefined value, based on Wagenführ (2006).
[b] For a 95% confidence, based on 36 bootstrapping-resamples.

Since it is not the actual value but the ratio between the two parameters that has an influence on the stress distribution in the cross section, the moduli of elasticity parallel and perpendicular to the grain were combined in a single parameter, which was assumed to be ($E_{t,0,ref}/E_{t,90,ref}$ =) 30 (Wagenführ, 2006). The reference tensile strength parallel to the grain ($f_{t,0,ref}$ = 180 MPa) and the reference tensile strength perpendicular to the grain ($f_{t,90,ref}$ = 7 MPa) were chosen according to Wagenführ (2006).

The calibration parameters were determined by minimising the residual sum of squares (RSS) between the estimated ($f_{t,0,estimated}$) and the experimentally determined tensile strengths ($f_{t,0,experimental}$) and are presented in Table 4. Only the training data set (n = 36) was considered in this procedure. The other 11 boards remained "unseen". Equation 7 results from this procedure. It can be used to estimate the tensile strength of a board based on the dynamic MOE (E_{dyn}), the minimum local tensile strength min($f_{t,ij}$), computed based on the local fibre direction (α_{ij}), and an error term ε. The independent variable min($f_{t,ij}$) alone, which is only based on the local fibre direction α_{ij}, shows a medium-high linear correlation with the logarithmic value of tensile strength ln(f_t) (R^2 = 0.65).

$$\ln(f_{t,0,estimated}) = 1.91 + 5.06 \cdot 10^{-5} \cdot E_{dyn} + 1.21 \cdot 10^{-2} \cdot \min(f_{t,ij}) + \varepsilon \quad (7)$$

Figure 8 summarises all process steps: based on photographs of the board sections (Figure 8a), the medullary ray spindles were identified (Figure 8b) and the field of fibre direction was generated (Figure 8c). The dynamic MOE (constant along the board) and the minimum local tensile strength of each cross sections i min($f_{t,j}$) are shown in Figure 8d. Such information on the tensile strength for each cross section / along the board's axis could be especially of importance for choosing the location of finger joints during fabrication. However, for the estimation of the tensile strength parallel to the grain of the board $f_{t,0,estimated}$, the lowest local tensile strength in the entire board min($f_{t,ij}$) is considered in Equation 7.

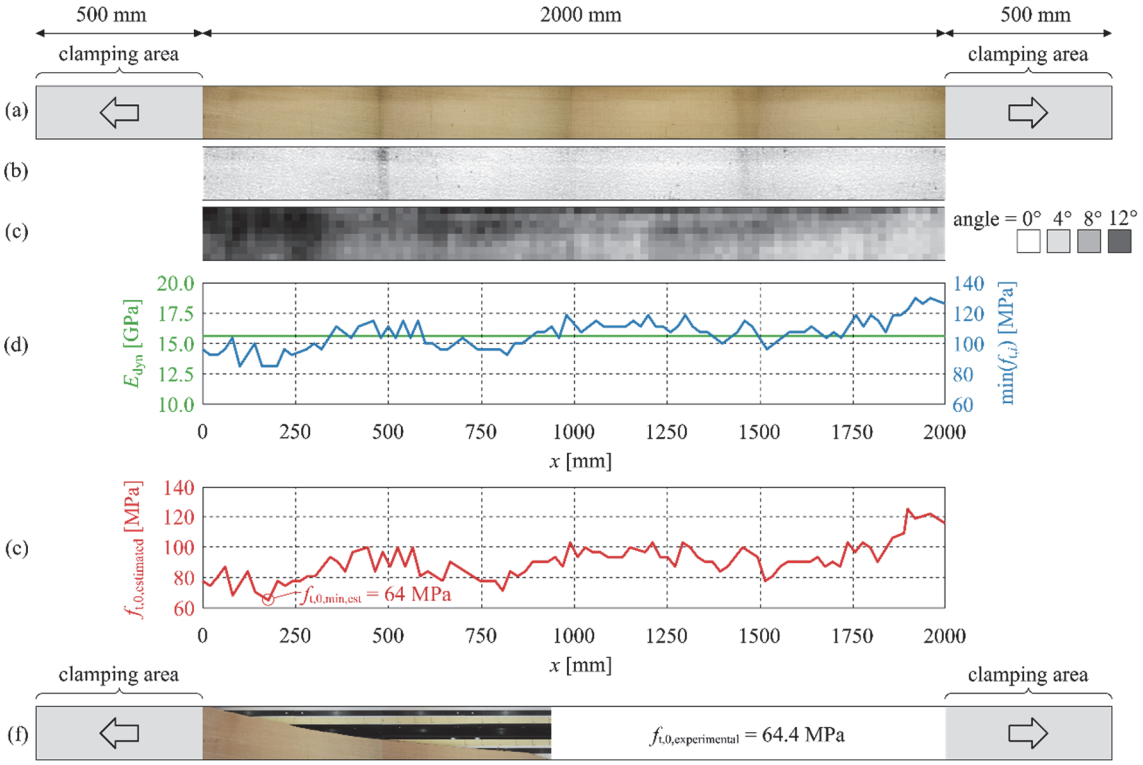

Figure 8 Overview of all steps of the reference model using the example of board no. 1035: photos of the board segments between the clamping jaws (a); post-processed black-and-white image of the medullary ray spindles (b); matrix of local fibre directions (c). Based on the measured E_{dyn} and min($f_{t,ij}$) along the board's longitudinal axis (d), the tensile strength $f_{t,0,estimated}$ is predicted (e). The fracture pattern (f) agrees well with the estimated fibre direction. The modelled ($f_{t,0,estimated}$ = 64 MPa; e) and experimentally determined tensile strength ($f_{t,0,experimental}$ = 64.4 MPa) are on a similar level and failure occurred in the area of maximum fibre inclination.

In Figure 9a, the tensile strength predicted by the developed model ($f_{t,0,estimated}$) is compared to the tensile strength determined in the destructive tension tests ($f_{t,0,experimental}$). A coefficient of determination of R^2 = 0.74 was found. The model error is described by a normally distributed error term (Fink, 2014) with the parameters $\varepsilon \sim N(\mu_\varepsilon = 0; \sigma_\varepsilon^2 = 0.018)$. Taking only the calibration data into account, the root mean square error (RMSE) of the model is 11.0 and the mean absolute percentage error (MAPE) of the model is 9.99.

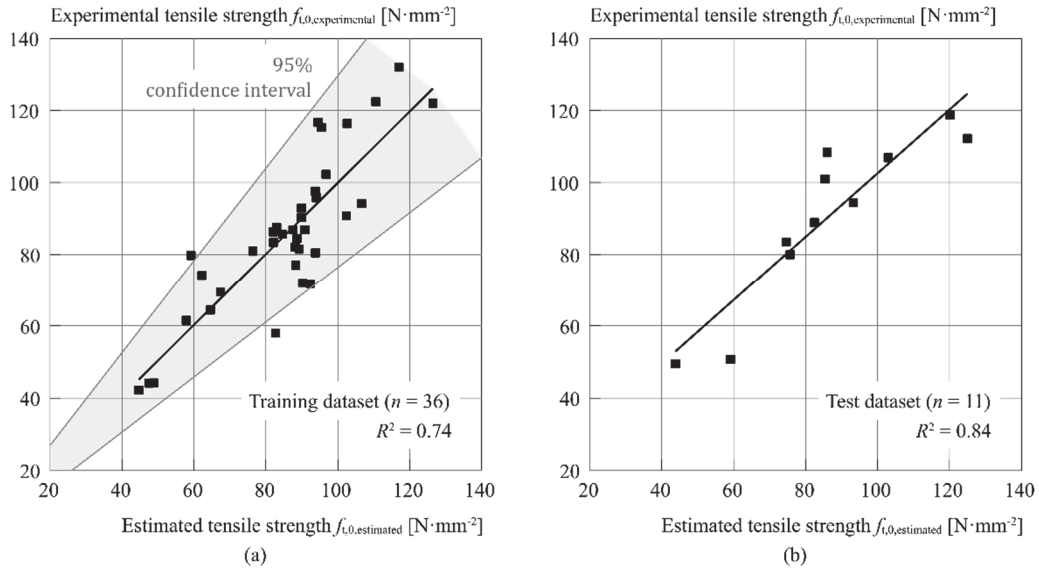

Figure 9 Correlation analysis between the modelled tensile strength $f_{t,0,estimated}$ and the experimentally determined tensile strength $f_{t,0,experimental}$ for the training data set (a) (n = 36; R^2 = 0.74) and the test data set (b) (n = 11; R^2 = 0.84).

In the training data set, the maximum deviation between the modelled and the experimentally determined tensile strength was found for board no. 2008 with a relative error of 43% (model: 82.8 MPa; experiment: 58.0 MPa). The predictions ($f_{t,0,estimated}$) for all other 35 boards lie within the 95% confidence interval and show a maximum deviation from the experimentally determined tensile strength ($f_{t,0,experimental}$) of ± 25%. For 22 of the 36 boards (61%), the relative error between modelled and experimentally determined tensile strength is below ± 10% (Figure 9). Applying the calibrated model to the (unseen) test data set reveals an even better coefficient of determination of R^2 = 0.84 (Figure 9b). Furthermore, the root mean square error (RMSE = 10.2) and the mean absolute percentage error (MAPE = 9.56) are lower compared to the training data set. A maximum relative difference between the experimentally determined and the modelled tensile strength for an individual board of 20% was observed. Although, the number of boards in the test data set was small (n = 11), these results indicate that even with unseen data the model is able to generate good estimates for the tensile strength parallel to the grain.

3.5 Comparison with models based on machine-learning techniques

The input parameters for the ML models were the two independent variables E_{dyn} and min($f_{t,ij}$) of each board. The density was not considered as an input parameter, since a preliminary check and the literature review indicated that the influence of this parameter on the strength of European beech wood was negligible (Table 3).

The deviation of the maximum and minimum values in the results obtained by different performance measures for each of the 6-folds for training and validating was very limited, indicating that all machine-learning models showed no tendency towards under- or overfitting (Table 5). Overfitting would mean that the analysis would correspond too closely to this particular set of data, without being able to predict subsequent (unseen) observations reliably. Theoretically, the prediction model works best when R^2 equals one and both RMSE and MAPE equal zero. Table 5 summarises the performance values R^2, RMSE and MAPE of the five models for the test data set, which was not considered in all prior analyses and therefore called ‘unseen’ in order to determine the generalisation ability of the models.

Table 5 Descriptive statistics for the training/validation data set (6-k cross-validation) and the test data set.

	Training/validation data set			Test data set		
Model	R^2	**RMSE**	**MAPE**[g]	R^2	**RMSE**	**MAPE**
Reference model	0.74	11.0	9.99	0.84	10.2	9.56
Support-Vector Machine[c]	0.71[a] ± 0.07[b]	11.5 ± 1.68	10.2 ± 2.15	0.87	8.40	7.72
Decision Tree[d]	0.83 ± 0.22	8.99 ± 2.86	7.79 ± 3.71	0.81	9.73	9.91
Random Forest[e]	0.87 ± 0.13	8.19 ± 2.30	7.13 ± 2.39	0.88	8.16	8.48
Artificial neural Network[f]	0.72 ± 0.07	11.4 ± 1.89	10.2 ± 2.75	0.86	8.46	7.59

[a] Selected model
[b] Standard deviation of the 6-k cross-validation
[c] MATLAB parameters: 'KernelFunction': linear; 'KernelScale': 2.18; 'IterationLimit': 1e6; 'Solver': SMO; 'BoxConstraint': 12635
[d] MATLAB parameters: 'MinParent': 10; 'MinLeaf: 1; 'MaxSplits': 29; 'PruneCriterion: mse; 'PredictorSelection': allsplit
[e] MATLAB parameters: 'Trees': 1000; 'mtry': 2/3; 'Sample size': size(Xtrain,1); 'Splitting rule': Randomly selected mtry; 'MinLeafSize': 2; 'NumPredictorsToSample:': 2
[f] MATLAB parameters: 'Architecture': 36-[5]-1; 'Training algorithm': Bayesian regularisation backpropagation; 'Transfer function': tansig (hidden layer), purelin (output layer); 'Epochs':5; 'Learning rate': 0.01
[g] Interpretation of the mean absolute percentage error (MAPE) according to Lewis (1982): MAPE ≤ 10% ↔ high accuracy prediction; 10% < MAPE ≤ 20% ↔ good prediction; 20% < MAPE ≤ 50% ↔ reasonable prediction; > 50% ↔ inaccurate prediction.

The results clearly show that the predictions of all machine-learning algorithms, according to the relevant indices (R^2, RMSE, MAPE), are highly correlated with the experimental observations of the mechanical tensile strength property (Table 5). When applied to the test data set, the predictive models Support-Vector Machine (R^2 = 0.87 / RMSE = 8.40 / MAPE = 7.72%) and Random Forest (R^2 = 0.88 / RMSE = 8.16 / MAPE = 8.48%) perform best, i.e., the predicted values were closest to the experimentally determined tensile strengths. The Artificial Neural Network model (R^2 = 0.86 / RMSE = 8.46 / MAPE = 7.59%) showed a similar prediction quality and performed best with regard to the MAPE. Even the worst performance of the machine-learning algorithms (Decision Tree algorithm) had acceptable accuracy indices of R^2 = 0.81, RMSE = 9.73 and MAPE = 9.91 for the test data set.

Due to the small dataset, the investigations were limited to the evaluation of the applicability of specific machine-learning techniques. The use of deep learning approaches, which require very large data sets and are computationally intensive, was not possible. This study shows that the reference model as well as shallow machine-learning algorithms can be used to analyse the limited dataset and to predict the tensile strength parallel to the grain of European beech boards with high accuracy. However, the use of shallow machine-learning algorithms on a small dataset required the use of cross-validation methods and holdout tests (Varma and Simon, 2006). As discussed above, efficient strength grading of timber is important when attempting at controlling the inherent heterogeneous material structure on different scales and the high variability of wood properties. Machine learning is a powerful tool in this respect and can help to overcome the recurring challenge in wood technology to transform the very heterogeneous raw material wood into products with high value and well defined properties (Schubert et al., 2020; Schubert and Kläusler, 2020).

4 Conclusion

The present study explores the potential of using information on the local fibre direction in addition to the dynamic modulus of elasticity in the strength grading process of European beech (*Fagus sylvatica* L.) boards. Based on investigations on 36 knot-free boards assigned to a training or calibration data set, which were used to train different machine-learning techniques (Support-Vector machines, Decision Tree, Random Forest, and Artificial Neural Network using a 6-k cross-validation approach), and another 11 boards assigned to the 'unseen' test data set, the following conclusions can be drawn:

- Data on the local fibre direction is very important for understanding and predicting the tensile strength parallel to the grain of European beech timber. Especially for knot-free boards this is considered the key parameter to achieve predictions of high accuracy.

- A model that takes into account the dynamic modulus of elasticity and a second parameter representing the critical local fibre direction was developed using a training data set (77% of the data). For this training data set, a coefficient of determination of $R^2 = 0.74$ between the predicted tensile strength and the experimentally determined tensile strength parallel to the grain and a mean absolute percentage error (MAPE) of 9.99% was found. Applying the model to the unseen test data set (23% of the data) showed an even better coefficient of determination of $R^2 = 0.84$ and a lower MAPE of 9.56%.
- Shallow machine-learning algorithms in combination with cross-validation methods were successfully used to further improve the prediction accuracy. The machine-learning techniques Support Vector Machine ($R^2 = 0.87$ / RMSE = 8.40 / MAPE = 7.7%) and Random Forest ($R^2 = 0.88$ / RMSE = 8.16 / MAPE = 8.5%) showed the best performance when applied to the unseen test data set.

The outcomes of this study indicate that the application of combined approaches, including experimental methods and machine-learning, have a great potential for increasing the precision of the strength grading of European beech timber. However, due to the limited size of the dataset available for this study, applying the presented methods to a larger dataset would be important and is envisaged in the course of follow-up projects. In the future, such combined approaches have the potential to contribute to a more resource-efficient use of this timber species widely available in Central Europe and may open new and more demanding fields for high-level timber applications.

Declarations

Funding

The authors wish to acknowledge the support of the Swiss Federal Office for the Environment FOEN within the framework of the Aktionsplan Holz [Projekt REF-1011-04200)].

Conflicts of interest/Competing interests

On behalf of all authors, the corresponding author states that there is no conflict of interest and that there are no competing interests.

Availability of data and material

In order to allow for transparency, verifiability and suggestions for further improvement of the presented methods, the following data will be made available for all 47 boards included in the study: Original images, processed images showing the identified medullary ray spindles, matrices of the local fibre directions, a table including information on the density, the dynamic and static MOE and the tensile strength parallel to the grain.

Code availability

Not applicable.

Author contributions

All authors contributed to the study conception and design. Material preparation, data collection and analysis were performed by Thomas Ehrhart, Pedro Palma and Mark Schubert. The first draft of the manuscript was written by Thomas Ehrhart, Pedro Palma, and Mark Schubert and all authors contributed to the following versions of the manuscript. All authors read and approved the final manuscript.

Consent to participate

Consent to participate has been received explicitly from all co-authors.

Consent to publication

Consent to publication has been received explicitly from all authors, as well as from the responsible authorities at the institutes where the work has been carried out.

References

Aicher S, Höfflin L, Behrens W (2001) A study on tension strength of finger joints in beech wood laminations. Otto-Graf-Journal 12:169–86.

Ashby MF, Easterling KE, Harrysson R, Maiti SK (1985) The fracture and toughness of woods. Proceedings of the Royal Society of London. Series A, Mathematical and Physical Sciences, 398:261-80. https://doi.org/10.1098/rspa.1985.0034

Baradit E, Aedo R, Correa J (2006) Knots detection in wood using microwaves. Wood Science and Technology 40(2):118–23. https://doi.org/10.1007/s00226-005-0027-8

Belkacemi M, Massich J, Lemaitre G, Stolz C, Daval V, Pot G, Aubreton O, Collet R, Meriaudeau F (2016) Wood fiber orientation assessment based on punctual laser beam excitation: A preliminary study. Proceedings of the 2016 International Conference on Quantitative Infrared Thermography (QIRT). Gdansk, Poland

Besseau B, Pot G, Collet R, Viguier J (2020) Influence of wood anatomy on fiber orientation measurement obtained by laser scanning on five European species. Journal of Wood Science, 66(1), 1-12. https://doi.org/10.1186/s10086-020-01922-y

Bishop CM (2006) Pattern recognition and machine learning. Information Science and Statistics. Springer-Verlag.

Blaß HJ., Denzler J, Frese M, Glos P, Linsenmann P (2005). Biegefestigkeit von Brettschichtholz aus Buche. Karlsruher Berichte zum Ingenieurholzbau - Band 1. Universitätsverlag Karlsruhe.

Brandner R, Schickhofer G (2008) Glued laminated timber in bending: New aspects concerning modelling. Wood Science and Technology 42:401-425. https://doi.org/10.1007/s00226-008-0189-2

Brännström M, Manninen J, Oja J (2008) Predicting the strength of sawn wood by tracheid laser scattering. BioResources 3(2):437–51.

Breiman L (2001) Random Forests. Machine Learning 45:5-32. https://doi.org/10.1023/A:1010933404324

Briggert A, Olsson A, Oscarsson J (2016) Three-dimensional modelling of knots and pith location in Norway spruce boards using tracheid-effect scanning. European Journal of Wood and Wood Products 74(5):725–39. https://doi.org/10.1007/s00107-016-1049-7

Cramer SM, McDonald KA (1989) Predicting lumber tensile stiffness and strength with local grain angle measurements and failure analysis. Wood and Fiber Science 21(1):393–410.

Curti R, Marcon B, Denaud L, Collet R (2018) Effect of grain direction on cutting forces and chip geometry during green beech wood machining. BioResources 13(3):5491–5503.

Daval V, Pot G, Belkacemi M, Meriaudeau F, Collet R (2015) Automatic measurement of wood fiber orientation and knot detection using an optical system based on heating conduction. Optics Express 23(26): 33529-33539. https://doi.org/10.1364/OE.23.033529

Denzler JK, Weidenhiller A (2015) Microwave scanning as an additional grading principle for sawn timber. European Journal of Wood and Wood Products 73(4):423–31. https://doi.org/10.1007/s00107-015-0906-0

DIN EN 408 (2012) Timber structures - Structural timber and glued laminated timber - Determination of some physical and mechanical properties. CEN.

DIN 4074-5 (2008) Strength grading of wood - Part 5 - Sawn hardwood. DIN.

DIN 4074-1 (2012) Strength grading of wood - Part 1 - Coniferous sawn timber. DIN.

Ehlbeck J, Colling F, Görlacher R (1985) Einfluss keilgezinkter Lamellen auf die Biegefestigkeit von Brettschichtholzträgern (Influence of finger-jointed laminaitons on the bending strength of glued laminated timber beams) (In German). Holz als Roh- und Werkstoff 43:333-337. https://doi.org/10.1007/BF02607817

Ehrhart T (2019) European beech glued laminated timber. PhD Thesis Nr. 26173. ETH Zürich. https://doi.org/10.3929/ethz-b-000402805

Ehrhart T, Fink G, Steiger R, Frangi A (2016a) Experimental investigation of tensile strength and stiffness indicators regarding European beech timber. World Conference on Timber Engineering. Vienna, Austria.

Ehrhart T, Fink G, Steiger R, Frangi A (2016b) Strength grading of European beech lamellas for the production of GLT and CLT. International Network on Timber Engineering Research, Meeting 49. Paper 49-5-1. Graz, Austria.

Ehrhart T, Steiger R, Frangi A (2018a) A non-contact method for the determination of fibre direction of European beech wood (*Fagus Sylvatica* L.). European Journal of Wood and Wood Products 76(3):925–935. https://doi.org/10.1007/s00107-017-1279-3

Ehrhart T, Steiger R, Palma P, Frangi A (2018b) Estimation of the tensile strength of European beech timber boards based on density, dynamic modulus of elasticity and local fibre orientation. World Conference on Timber Engineering (WCTE 2018), Seoul, Republic of Korea.

Fathi H, Nasir V, Kazemirad S (2020) Prediction of the mechanical properties of wood using guided wave propagation and machine learning. Construction and Building Materials 262(120848). https://doi.org/10.1016/j.conbuildmat.2020.120848

Federal Office for the Environment FOEN (2018) Swiss statistical yearbook of forestry (Jahrbuch Wald und Holz - Annuaire La forêt et le bois). UZ Nr. 1830, FOEN, Bern, Switzerland (in German and French).

Fink G (2014) Influence of varying material properties on the load-bearing capacity of glued laminated timber. PhD Thesis Nr. 21746. ETH Zürich. https://doi.org/10.3929/ethz-a-010108864

Foley C (2001) A three-dimensional paradigm of fiber orientation in timber. Wood Science and Technology 35(5):453–65. https://doi.org/10.1007/s002260100112

Frese M (2006) Bending strength of beech glued laminated timber (in German). PhD Thesis. Universität Karlsruhe, Germany.

Frühwald A, Ressel JB, Bernasconi A, Becker P, Pitzner B, Wonnemann R, Mantau U, Sörgel C, Thoroe C, Dieter M, Englert H (2003). Hochwertiges Brettschichtholz aus Buchenholz. Forschungsprojekt – Abschlussbericht (High-quality glued laminated timber made of beech wood. Research project – Final report) (in German). Bundesforschungsanstalt für Forst- und Holzwirtschaft, Hamburg, Germany.

Frühwald K, Schickhofer G (2005) Strength grading of hardwoods. Proceedings of the 14th International Symposium on Nondestructive Testing of Wood, 198-208. Hannover, Germany.

Glos P, Lederer B (2000) Sortierung von Buchen- und Eichenschnittholz nach der Tragfähigkeit und Bestimmung der zugehörigen Festigkeits- und Steifigkeitskennwerte (Sorting of beech and oak sawn timber according to the load-bearing capacity and determination of the associated strength and stiffness properties) (in German). TU München, Holzforschung München (internal report no. 98508), Munich, Germany.

Hankinson RL (1921) Investigation of crushing strength of spruce at varying angles of grain. Air Force Information Circular No. 259, U. S. Air Service.

Hinton GE, Salakhutdinov RR (2006) Reducing the dimensionality of data with Neural Networks. Science 313:504-507. https://doi.org/10.1126/science.1127647

Hübner U (2013) Mechanische Kenngrößen von Buchen-, Eschen- und Robinienholz für lastabtragende Bauteile (Mechanical properties of beech, ash and black locust wood for load-carrying members) (in German). PhD Thesis. Graz University of Technology. http://dx.medra.org/10.3217/978-3-85125-314-6

JCSS (2006) JCSS Probabilistic Model Code. Part III – Resistance models. Properties of timber. In: JCSS Probabilistic Model Code. Joint Committee on Structural Safety, p 16

Jungo N (2016) Investigations on indicating parameters for the strength properties of beech wood (in German). Master Project Thesis. ETH Zürich.

Kohavi R (1995) A study of cross-validation and bootstrap for accuracy estimation and model selection. Proceedings of the 14th International Joint Conference on Artificial Intelligence. Volume 21995, p. 1137-1143. Morgan Kaufmann Publishers Inc.: Montreal, Quebec, Canada.

Kotsiantis SB (2013). Decision trees: a recent overview. Artificial Intelligence Review 39:261–283. https://doi.org/10.1007/s10462-011-9272-4

Krapez JC, Gardette G, Balageas DL (1996) Thermal ellipsometry in steady-state and by lock-in thermography: Application to anisotropic materials characterization. Proceedings of Quantitative Infrared Thermography QIRT 96 Eurotherm Seminar 50 257–62. http://dx.doi.org/10.21611/qirt.1996.042

LeCun Y, Bengio Y, Hinton G (2015) Deep learning. Nature 521:436-444.https://doi.org/10.1038/nature14539

Lewis CD (1982) Industrial and business forecasting methods. Butterworths, London, UK. https://doi.org/10.1002/for.3980020210

Lukacevic M, Füssl J (2014) Numerical simulation tool for wooden boards with a physically based approach to identify structural failure. European Journal of Wood and Wood Products 72(4):497–508. https://doi.org/10.1007/s00107-014-0803-y

Mansfield S D, Iliadis L, Avramidis S (2007) Neural network prediction of bending strength and stiffness in western hemlock (*Tsuga heterophylla* Raf.). Holzforschung 61:707-716. https://doi.org/10.1515/HF.2007.115Matthews PC, Beech BH (1976) US Patent 3,976,384: Method and apparatus for detecting timber defects.

Matthews PC, Soest JF (1986) US Patent 4,606,64: Method for determining localized fiber angle in a three dimensional fibrous material.

Metcalfe L, Dashner B (2002) US Patent 2002/0025061A1: High speed and reliable determination of lumber quality using grain influenced distortion effects.

Norimoto M, Yamada T (1972) The dielectric properties of wood VI: On the dielectric properties of the chemical constituents of wood and the dielectric anisotropy of wood. Wood Research: Bulletin of the Wood Research Institute Kyoto University, 52:31–43. http://hdl.handle.net/2433/53414

Norton JAP, McLaughlan TA, Kusec DJ (1974) US Patent 3,805,156: Wood slope of grain indicator.

Nyström J (2003) Automatic measurement of fiber orientation in softwoods by using the tracheid effect. Computers and Electronics in Agriculture 41(1–3):91–99. https://doi.org/10.1016/S0168-1699(03)00045-0

Olsson A, Pot G, Viguier J, Faydi Y, Oscarsson J (2018) Performance of strength grading methods based on fibre orientation and axial resonance frequency applied to Norway spruce (*Picea abies L.*), Douglas fir (*Pseudotsuga menziesii (Mirb.) Franco*) and European oak (*Quercus petraea* (Matt.) Liebl./*Quercus robur* L.). Annals of Forest Science, 75(4), 1-18. https://doi.org/10.1007/s13595-018-0781-z

Olsson A, Oscarsson J (2017) Strength grading based on high resolution laser scanning and dynamic excitation: A full scale investigation of performance. European Journal of Wood and Wood Products 75(1):17–31. https://doi.org/10.1007/s00107-016-1102-6

Olsson A, Oscarsson J, Serrano E, Källsner B, Johansson M, Enquist B (2013) Prediction of timber bending strength and in-member cross-sectional stiffness variation on the basis of local wood fibre orientation. European Journal of Wood and Wood Products 71(3):319–33. https://doi.org/10.1007/s00107-013-0684-5

Ohnesorge D, Richter K, Becker G (2010). Influence of wood properties and bonding parameters on bond durability of European Beech (*Fagus sylvatica* L.) glulams. Ann. For. Sci. 67, 601. https://doi.org/10.1051/forest/2010002

Plos M, Fortuna B, Straze A, Turk G (2018) Visual grading of beech wood - a decision tree approach. World Conference on Timber Engineering. Seoul, Republic of Korea.

671 Ridley-Ellis D, Stapel P, Baño V (2016) Strength grading of sawn timber in Europe: an explanation for
672 engineers and researchers. Eur J Wood Prod 74:291–306. https://doi.org/10.1007/s00107-016-1034-1

673 Sarén MP, Serimaa R, Tolonen Y (2006) Determination of fiber orientation in Norway Spruce using X-
674 ray diffraction and laser scattering. European Journal of Wood and Wood Products 64(3):183–88.
675 https://doi.org/10.1007/s00107-005-0076-6

676 Sarnaghi AK, van de Kuilen JWG (2019) Strength prediction of timber boards using 3D FE-analysis.
677 Construction and Building Materials 202:563-573. https://doi.org/10.1016/j.conbuildmat.2019.01.032

678 Sauter UH, Breinig L (2016) European hardwoods for the building sector: Reality of today - Possibilities
679 for tomorrow, WP 1 - Hardwood resources in Europe: Standing stock and resource forecasts. Workshop
680 Garmisch-Partenkirchen, Germany.

681 Schindelin J, Arganda-Carreras I, Frise E, Kaynig V, Longair M, Pietzsch T, Preibisch S, Rueden C,
682 Saalfeld S, Schmid B, Tinevez JY, White DJ, Hartenstein V, Eliceiri K, Tomancak P, Cardona A (2012)
683 Fiji: an open-source platform for biological-image analysis. Nature Methods 9(7):676-682.
684 https://doi.org/10.1038/nmeth.2019

685 Schubert M, Kläusler O (2020) Applying machine learning to predict the tensile shear strength of bonded
686 beech wood as a function of the composition of polyurethane prepolymers and various pretreatments.
687 Wood Science and Technology 54:19-29. https://doi.org/10.1007/s00226-019-01144-6

688 Schubert M, Luković M, Christen H (2020) Prediction of mechanical properties of wood fiber insulation
689 boards as a function of machine and process parameters by random forest. Wood Science and Technology
690 54:703–713. https://doi.org/10.1007/s00226-020-01184-3

691 Schlotzhauer P, Wilhelms F, Lux C, Bollmus S (2018) Comparison of three systems for automatic grain
692 angle determination on European hardwood for construction use. European Journal of Wood and Wood
693 Products 76(3):911-23. https://doi.org/10.1007/s00107-018-1286-z

694 Simonaho SP, Palviainen J, Tolonen Y, Silvennoinen R (2004) Determination of wood grain direction
695 from laser light scattering pattern. Optics and Lasers in Engineering 41(1):95–103.
696 https://doi.org/10.1016/S0143-8166(02)00144-6

697 Snoek J, Larochelle H, Adams RP (2012) Practical Bayesian optimization of machine learning
698 algorithms. Proceedings of the 25th International Conference on Neural Information Processing Systems -
699 Volume 2 2012, Curran Associates Inc.: Lake Tahoe, Nevada. p. 2951-2959.

700 Soest JF (1997) US Patent 5,703,960: Lumber defect scanning including multi-dimensional pattern
701 recognition.

702 Steele PH, Neal SC, McDonald SM (1991) The slope-of-grain indicator for defect detection in unplaned
703 hardwood lumber. Forest Products Journal 41(1):15–20.

704 Vapnik VN (1995) The nature of statistical learning theory. Springer-Verlag. https://doi.org/10.1007/978-
705 1-4757-3264-1

706 Varma S, Simon R (2006) Bias in error estimation when using cross-validation for model selection. BMC
707 Bioinformatics 7, 91. https://doi.org/10.1186/1471-2105-7-91

708 Viguier J, Bourgeay C, Rohumaa A, Pot G, Denaud L (2018). An innovative method based on grain angle
709 measurement to sort veneer and predict mechanical properties of beech laminated veneer lumber.
710 Construction and Building Materials, 181, 146-155. https://doi.org/10.1016/j.conbuildmat.2018.06.050

711 Viguier J, Bourreau D, Bocquet JF, Pot G, Bléron L, Lanvin JD (2017) Modelling mechanical properties
712 of Spruce and Douglas Fir timber by means of X-ray and grain angle measurements for strength grading
713 purpose. European Journal of Wood and Wood Products 75(4):527–41. https://doi.org/10.1007/s00107-
714 016-1149-4

715 Viguier J, Jehl A, Collet R, Bleron L, Meriaudeau F (2015) Improving strength grading of timber by grain
716 angle measurement and mechanical modeling. Wood Material Science and Engineering 10(1):145–56.
717 https://doi.org/10.1080/17480272.2014.951071

718 Wagenführ R (2006) Holzatlas (in German). 6th Edition. Carl Hanser Verlag, Dresden, Germany:

719 Weidenhiller A, Linsenmann P, Lux C, Brüchert F (2019) Potential of microwave scanning for
720 determining density and tension strength of four European hardwood species. European Journal of Wood
721 and Wood Products 77(2):235–47. https://doi.org/10.1007/s00107-019-01387-x

722 Westermayr M, Stapel P, Van de Kuilen JWG (2018) Tensile and compression strength of small cross
723 section beech glulam members. International Network on Timber Engineering Research, Meeting 51.
724 Paper 51-12-2. Tallinn, Estonia.